Low Temperature Physics/Fizika Nizkikh Temperatur, 2020, vol. 46, No. 12, pp. 1430–1436

First-principles LCAO study of the low- and room-temperature phases of $CdPS_3$

Alexei Kuzmin

Institute of Solid State Physics, University of Latvia, Riga LV-1063, Latvia
E-mail: a.kuzmin@cfi.lu.lv

Received September 24, 2020, published online October 21, 2020

The electronic and atomic structure of a bulk 2D layered van-der-Waals compound $CdPS_3$ was studied in the low ($R3$) and room ($C2/m$) temperature phases using first-principles calculations within the periodic linear combination of atomic orbitals method with hybrid meta exchange-correlation M06 functional. The calculation results reproduce well the experimental crystallographic parameters. The value of the indirect band gap E_g = 3.4 eV for the room-temperature monoclinic $C2/m$ phase is close to the experimental one, while the indirect band gap E_g = 3.3 eV was predicted for the low-temperature trigonal $R3$ phase. The effect of hydrostatic pressure on the band gap in both phases was studied in the pressure range from 0 to 40 GPa. In both cases, the pressure dependence of the band gap passes through a maximum, but at different pressures. In the $R3$ phase, the band gap reaches its maximum value of ~ 4 eV at ~ 30 GPa, whereas in the $C2/m$ phase, the maximum value of ~ 3.6 eV is reached already at ~ 8 GPa.

Keywords: $CdPS_3$, layered compound, electronic structure, first-principles calculations, high pressure.

1. Introduction

Two-dimensional (2D) layered compounds represent a rich class of functional materials with tunable electronic, magnetic and optical properties [1–3]. Their atomic structure is distinguished by strong in-plane bonding and weak van-der-Waals (vdW) out-of-plane interactions, which make it possible to exfoliate the material into 2D (single-)layers and pack them into heterostructures [4, 5]. More than a few hundred 2D layered materials are known today, while more than five thousand such compounds were predicted by high-throughput first-principles calculations [6].

Among different groups of 2D layered materials, metal thio(seleno)phosphates (MTPs), being moderate- to wide-bandgap semiconductors, represent a particular interest [7]. Their crystallographic structure (Fig. 1) consists of the $[P_2S(Se)_6]^{4-}$ anion framework forming slabs, staking along the c-axis and stabilized by metal cations, which can be group I and II elements, most of the transition metals, some heavier metals as well as a few lanthanides and actinides [7]. It is the type of metal cation that is responsible for a wide variety of the MTP functionalities. While MTP materials are currently a hot topic of research, some of them were less studied. Here the case of $CdPS_3$ will be discussed.

At room temperature, $CdPS_3$ crystallizes in the monoclinic $C2/m$ (No. 12) phase with two formula units in the primitive unit cell, but with four formula units in the crystallographic unit cell [8–10]. The atoms occupy the following Wyckoff positions: Cd 4g(0, y, 0), P 4i(x, 0, z), S1 4i(x, 0, z), S2 8j(x, y, z) (Table 1). The experimental band gap E_g is equal to 2.95 eV [11], 3.06 eV [12], and 3.5 eV [13–15], which makes it possible to classify $CdPS_3$ as a wide-bandgap semiconductor.

When the temperature drops below 228 K, $CdPS_3$ transforms into the low-temperature trigonal $R3$ (No. 146) phase with two formula units in the primitive unit cell, but with six formula units in the crystallographic unit cell [16–18]. The atoms are located at the following Wyckoff positions: Cd1 3a(0, 0, z), Cd2 3a(1/3, 2/3, z), P1 3a(2/3, 1/3, z), P2 3a(2/3, 1/3, z), S1 9b(x, y, z), S2 9b(x, y, z) (Table 1). To our knowledge, the experimental value of the band gap for the $R3$ phase has not been reported.

The layered structure of $CdPS_3$ can also be characterized by the interlayer spacings (vdW gaps) and the layer thickness, defined as the distance between the planes containing sulfur atoms on opposite sides of the layer (Fig. 1). The experimental interlayer spacings and the layer thicknesses are close in both phases and are, respectively, equal to ~ 3.12 Å and ~ 3.37 Å for the $R3$ phase [3] and to ~ 3.16 Å and ~ 3.38 Å for the $C2/m$ phase [9, 10].

Most recent theoretical studies of $CdPS_3$ have used the plane-wave DFT approach [19–21].

The band gap E_g equal to 2.96 eV was obtained for bulk $CdPS_3$ and 3.03 eV for its single-layer in [19] using a hybrid HSE06 exchange-correlation functional [22]. It was

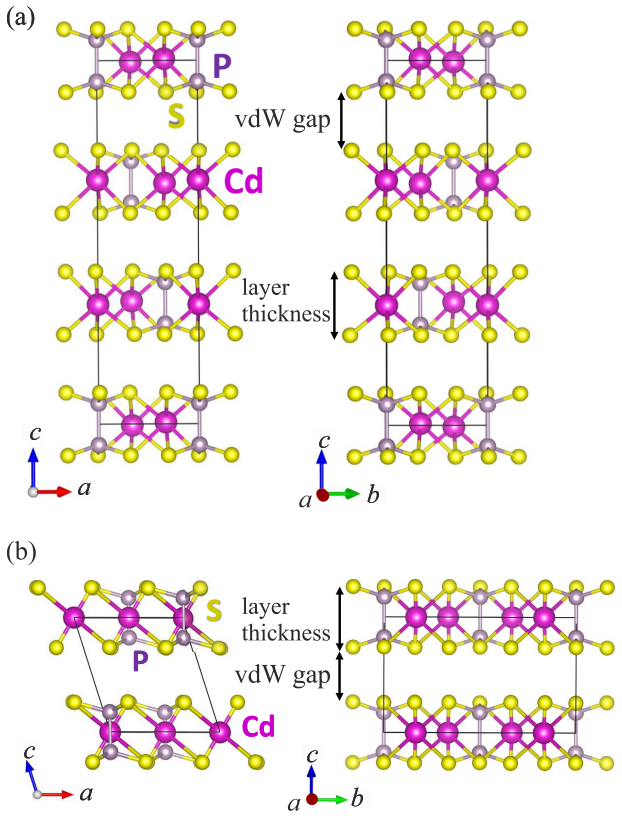

Fig. 1. (Color online) Crystallographic structure of $CdPS_3$ in the low-temperature trigonal *R*3 [17] (a) and room-temperature monoclinic *C*2/*m* [8, 9] phases (b) at pressure $P = 0$ GPa. The interlayer spacings (vdW gaps) between neighbouring layers and the layer thicknesses are indicated. The illustrations were created using the VESTA software [36].

concluded that the electronic structure of single-layer $CdPS_3$ is suitable for visible-light driven photocatalysis, and the position of its band edges relative to the water redox potential makes single-layer $CdPS_3$ a promising candidate for photocatalytic splitting of water [19].

Vibrational properties of MTPs were studied in [21] using the generalized gradient approximation (GGA) for the exchange-correlation energy in the form of the PBE functional [23]. While the structure of $CdPS_3$ was satisfactory reproduced, the calculated band gap value of 1.93 eV was underestimated compared to the known experimental values. The calculated Raman active modes were analysed in detail for the unstrained and strained layers, and the frequency shifts of the modes in response to biaxial strain were determined [21]. The computed elastic properties indicated that MTPs (including $CdPS_3$) have very soft lattice compared to other layered materials (e.g., MoS_2 and graphene) [21].

The effect of strain on the electronic structure of MPX_3 (M = Zn, Cd; X = S, Se) single-layers was also studied in [20]. It was found that $CdPS_3$ always has indirect band gap under the strain load of up to ± 10%. Moreover, under the compressive strain, the band gaps of MPX_3 single-layers increase firstly and then decrease, whereas the tensile strain leads only to a decrease of the band gaps. It was concluded

Table 1. Crystallographic parameters, atomic displacement parameters (ADPs) B_{eq} (at 133 K for *R*3 and 298 K for *C*2/*m* phases) and band gap E_g values for $CdPS_3$ in low-temperature *R*3 and room-temperature *C*2/*m* phases

	Space group *R*3 (146)		Space group *C*2/*m* (12)	
	Experiment [17]	LCAO	Experiment [9, 10]	LCAO
a, Å	6.224	6.189	6.218	6.167
b, Å			10.763	10.690
c, Å	19.490	18.784	6.867	6.752
β, grad			107.58	107.72
y(Cd1)			0.3322	0.3324
z(Cd1)	0.3291	0.3301		
z(Cd2)	0.3380	0.3368		
x(P1)			0.0551	0.0575
z(P1)	0.3900	0.3930	0.1698	0.1741
z(P2)	0.2757	0.2739		
x(S1)	0.3450	0.3416	0.7686	0.7618
y(S1)	0.3214	0.3266		
z(S1)	0.4201	0.4225	0.2541	0.2582
x(S2)	–0.0168	–0.0083	0.2401	0.2467
y(S2)	0.3422	0.3401	0.1567	0.1610
z(S2)	0.2471	0.2443	0.2584	0.2628
B_{eq}(Cd), Å^2	0.856	0.31	1.84	0.67
B_{eq}(P), Å^2	0.54	0.19	0.91	0.34
B_{eq}(S), Å^2	0.65	0.27	1.23, 1.28	0.52, 0.55
E_g, eV		3.3	2.95 eV [11] 3.06 [12] 3.5 [13–15]	3.4

that the MPX_3 single-layers are promising candidates for the tunable electronic structures by strain engineering [20].

In this study, the electronic structure of the low (*R*3) and room (*C*2/*m*) temperature phases of bulk $CdPS_3$ was studied using first-principles linear combination of atomic orbitals (LCAO) method, and the effect of hydrostatic pressure on the band gap in both phases was evaluated.

2. Methodology

First-principles calculations of $CdPS_3$ were performed by the linear combination of LCAO method using the CRYSTAL17 code [24]. The basis sets for P, S and Cd atoms were chosen in the form of all-electron triple-zeta valence (TZV) basis sets augmented by one set of polarization functions (pob-TZVP) [25].

The evaluation of the Coulomb and exchange series was done with the accuracy controlled by a set of tolerances, which were selected to be (10^{-8}, 10^{-8}, 10^{-8}, 10^{-8}, 10^{-16}). The Monkhorst–Pack scheme [26] for an 8×8×8 *k*-point

mesh was used to integrate the Brillouin zone. The SCF calculations were performed employing the M06 [35] functional with a 10^{-10} tolerance for the total energy change.

The lattice parameters and atomic fractional coordinates were optimized for the low-temperature trigonal $R3$ [17] and room-temperature monoclinic $C2/m$ [9, 10] $CdPS_3$ phases. The atomic charges were estimated from the Mulliken population analysis [28]. The calculated lattice parameters (a, b, c, β), atomic fractional coordinates (x, y, z) and the values of the band gap E_g are reported in Table 1.

Calculated band structures and total/projected density of states (DOS) are shown in Figs. 2–4. The band structures were calculated along band paths in the Brillouin zone chosen according to [29]. Note that in the rhombohedral space group $R3$, belonging to the trigonal crystal system, two topologically different shapes of the Brillouin zone (and, respectively, sets of the high-symmetry points) are possible depending on the ratio between a and c lattice parameters [29, 30]. In our case $\sqrt{3}a < \sqrt{2}c$ (Table 1), and the Brillouin zone has the topology of the truncated octahedron [30].

Additionally to structural parameters, the atomic displacement parameters B_{eq} were determined for the $R3$ phase at 133 K and for the $C2/m$ phase at 298 K in order to compare them with the available experimental data (Table 1). ADPs were calculated in the harmonic approximation for the supercell size 2×2×1 from the eigenvalues and eigenvectors of the dynamic matrix [31], which was obtained using the direct (frozen-phonon) method [24, 32].

Finally, the lattice parameters and atomic fractional coordinates were optimized at several selected pressures in the range of 0–40 GPa for the $R3$ and $C2/m$ phases of $CdPS_3$. The structure optimization at the required pressure was performed using the approach developed in [33]. Total and projected onto the set of atomic orbitals density of states at selected pressures are presented in Fig. 4. Pressure dependences of the primitive cell volume $V(P)$ and the band gap $E_g(P)$ are shown in Fig. 5.

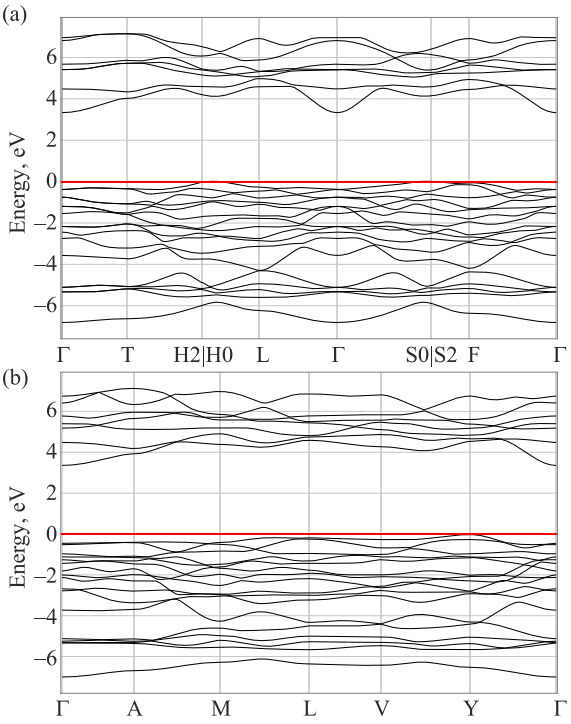

Fig. 2. Band structure diagrams of $CdPS_3$ for the low-temperature trigonal $R3$ (a) and room-temperature monoclinic $C2/m$ phases (b) at $P = 0$ GPa. The energy zero is set at the top of the valence band (Fermi energy position).

3. Results and discussion

The structural properties of bulk $CdPS_3$ from our LCAO calculations agree with the experimental findings for both low- and room-temperature phases (Table 1). The obtained values of the Mulliken charges for three ions are close in both phases and are equal to Z(Cd) = +0.61, Z(P) = +0.17 and Z(S) = –0.26. The indirect band gap was found in both phases (Fig. 2). Its value E_g = 3.4 eV for the $C2/m$ phase is close to the experimental ones, ranging from 2.95 to 3.5 eV [11–15]. The experimental data for the band gap in the $R3$

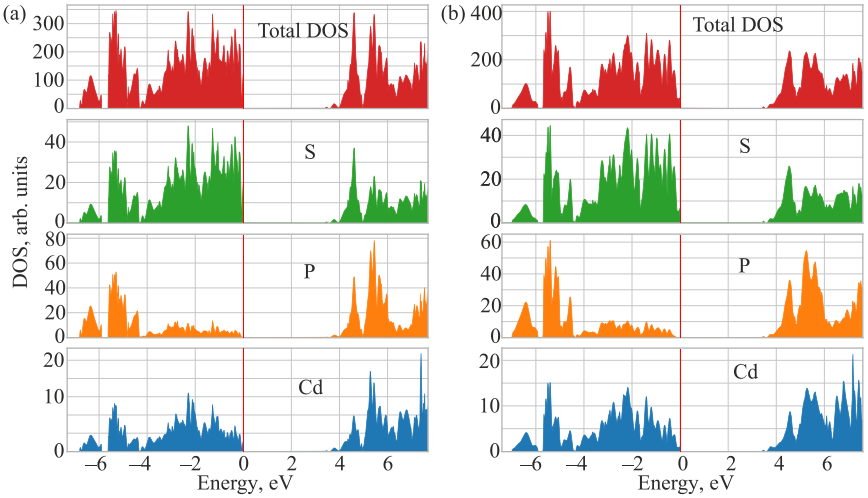

Fig. 3. (Color online) Total and projected onto atoms DOS for the low-temperature trigonal $R3$ (a) and room-temperature monoclinic $C2/m$ $CdPS_3$ phases (b) at $P = 0$ GPa. The energy zero is set at the top of the valence band (Fermi energy position).

phase are not available to our knowledge, and our calculations predict a value of 3.3 eV.

The atomic displacement parameters B_{eq} (Table 1) were used to estimate the amplitude of thermal vibrations of atoms in harmonic approximation. The calculations were carried out at two temperatures (133 K for the *R*3 phase and 298 K for the *C*2/*m* phase), for which the experimental data [9, 10, 17] are available. Comparison of the calculated

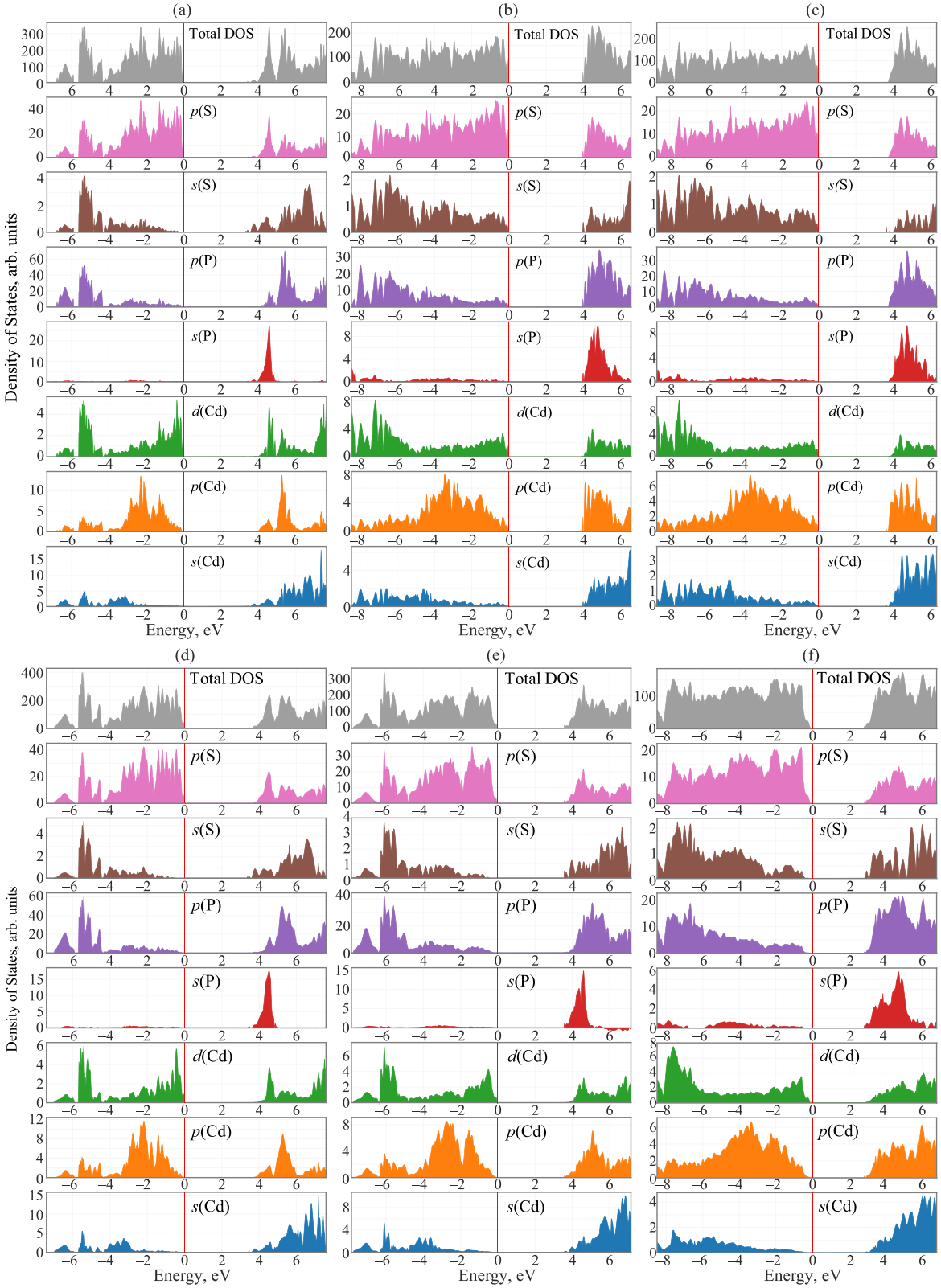

Fig. 4. (Color online) Total and projected onto the set of atomic orbitals DOS in $CdPS_3$ for the low-temperature trigonal *R*3 phase at 0 (a), 30 (b) and 40 (c) GPa and room-temperature monoclinic *C*2/*m* phases at 0 (d), 8 (e) and 40 (f) GPa. The energy zero is set at the top of the valence band (Fermi energy position).

and experimental ADP values for Cd, P and S atoms shows that the theoretical values are systematically lower. Nevertheless, the relative ADP values (larger for Cd and smaller for P) are reproduced. The large values of the experimental ADPs for Cd atoms were attributed in the past to their apparent off-center displacement caused by a second-order Jahn–Teller effect [10, 34].

The total density of states (DOS) and its projection onto atoms (Fig. 3) and onto a set of atomic orbitals (the *s*, *p* and *d* orbitals of Cd, P and S atoms) (Fig. 4) allow us to draw a conclusion about the nature of electronic states in the valence and conduction bands.

As one can see, there is no big difference in DOSs for the *R*3 and *C*2/*m* phases at 0 GPa. The valence band maximum is dominated by 3*p*(S) orbitals with much lower contribution from 4*d*(Cd) and 3*p*(P) orbitals. The conduction band minimum is mainly comprised of the 3*p*(S), 3*s*(P) and 3*p*(P) orbitals with some admixture of the 5*s*(Cd) and 3*s*(S) orbitals. The important role of the 3*p*(P) states at the bottom of the conduction band was demonstrated recently in $FePS_3$ [9].

An increase in pressure has a similar effect on the density of states in the *R*3 and *C*2/*m* phases. The contribution of the 5*p*(Cd) orbitals appears at the bottom of the conduction band in addition to the contributions of the 3*p*(S), 3*s*(P), 3*p*(P), 5*s*(Cd) and 3*s*(S) orbitals. At largest pressures, the edges of the valence and conduction bands broaden, which leads to a decrease in the band gap.

The effect of pressure on the $CdPS_3$ structure is shown in Fig. 5. Compression leads to a gradual reduction in the volume of the primitive cell in both phases, however, the pressure dependence of the band gap passes through a maximum, but at different pressures. The band gap increases almost linearly in the *R*3 phase reaching a maximum value of ~ 4 eV at ~ 30 GPa and then decreases, while in the *C*2/*m* phase, the maximum value of the band gap of ~ 3.6 eV is observed at ~ 8 GPa.

Pressure dependence of the interatomic distances is summarized in Table 2 at three selected pressures. The calculations show that upon compression all interatomic distances are reduced, but in different ways. In the *R*3 phase, Cd atoms coordinated octahedrally by S atoms displace along the *c*-axis direction upon increasing pressure, so that the CdS_6 octahedra become more distorted at 30 GPa. In the *C*2/*m* phase,

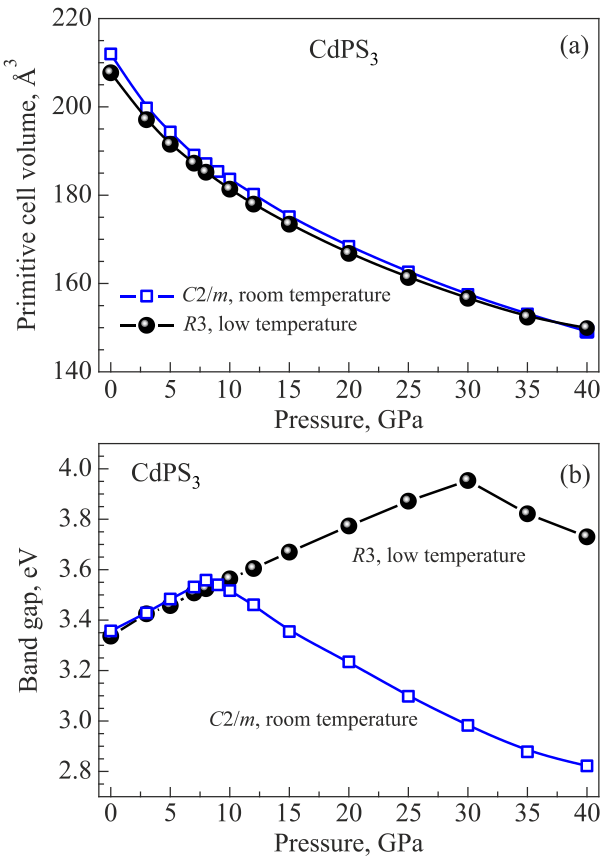

Fig. 5. Pressure dependence of the calculated primitive cell volume (a) and the band gap E_g (b) for the low-temperature trigonal *R*3 and room-temperature monoclinic *C*2/*m* $CdPS_3$ phases.

Table 2. Pressure dependence of the calculated interatomic distances in $CdPS_3$ in low-temperature *R*3 and room-temperature *C*2/*m* phases at three selected pressures. The difference Δ between the distances at 30 and 0 GPa is shown in the last column

	0 GPa	8 GPa	30 GPa	Δ
		*R*3 phase		
Cd–S	2.67	2.60	2.49	–0.18
	2.70	2.65	2.57	–0.13
⟨Cd–S⟩	2.69	2.63	2.53	–0.16
P–S	2.07	2.05	2.00	–0.06
P–P	2.24	2.20	2.13	–0.11
Cd–Cd	3.58	3.49	3.34	–0.23
Cd–P	3.73	3.62	3.44	–0.28
	3.76	3.69	3.55	–0.22
⟨Cd–P⟩	3.75	3.66	3.50	–0.25
		*C*2/*m* phase		
Cd–S	2.67	2.60	2.50	–0.17
	2.68	2.61	2.51	–0.17
	2.70	2.65	2.54	–0.16
⟨Cd–S⟩	2.68	2.62	2.52	–0.17
P–S	2.07	2.04	2.00	–0.07
P–P	2.24	2.21	2.16	–0.08
Cd–Cd	3.55	3.43	3.20	–0.36
	3.58	3.52	3.43	–0.15
⟨Cd–Cd⟩	3.57	3.47	3.31	–0.25
Cd–P	3.73	3.61	3.41	–0.32
	3.74	3.64	3.47	–0.27
⟨Cd–P⟩	3.73	3.63	3.44	–0.30

their displacement is much smaller and occurs along the *b*-axis direction, so that the CdS_6 octahedra are distorted less.

Different displacements of Cd atoms in the *R*3 and *C*2/*m* phases have different effects on the Cd–Cd and Cd–P interatomic distances. In both phases, their mean values decrease, respectively, by 0.23–0.25 Å and 0.25–0.30 Å upon compression. However, only in the *C*2/*m* phase there are two different Cd–Cd distances of about 3.55 Å and 3.58 Å at 0 GPa, and their difference increases at 30 GPa up to 0.23 Å (the distances are 3.20 Å and 3.43 Å). The Cd–P distribution is split in both phases, and the splitting increases from 0.01–0.03 Å at 0 GPa to 0.07–0.11 Å at 30 GPa.

The interatomic P–S distances are reduced by 0.07 Å in both phases under compression from 0 to 30 GPa. Similar behavior is observed for the P–P distances in the P_2S_6 group: they are reduced, respectively, by 0.11 Å and 0.08 Å in the *R*3 and *C*2/*m* phases at 30 GPa.

4. Conclusions

A detailed investigation of the electronic and atomic structure of a bulk 2D layered van-der-Waals compound $CdPS_3$ was performed in the low-temperature (*R*3) and room-temperature (*C*2/*m*) phases using first-principles LCAO calculations with hybrid M06 exchange-correlation functional. The obtained results agree with the known experimental crystallographic parameters. Close indirect band gaps of 3.3 and 3.4 eV were found for the *R*3 and *C*2/*m* phases at 0 GPa, respectively. At the same time, the band gap has a pronounced dependence on pressure with a maximum value at pressures that differ in the two phases. Hence, pressure can be used to modulate the electronic structure of bulk $CdPS_3$.

Acknowledgements

A.K. is grateful to the Latvian Council of Science project No. lzp-2018/2-0353 for financial support. Institute of Solid State Physics, University of Latvia as the Center of Excellence has received funding from the European Union's Horizon 2020 Framework Programme H2020-WIDESPREAD-01-2016-2017-TeamingPhase2 under grant agreement No. 739508, project CAMART2.

1. A. Gupta and T. Sakthivel, and S. Seal, *Prog. Mater. Sci.* **73**, 44 (2015).
2. R. Lv, H. Terrones, A. L. Elías, and N. Perea-López, H. R. Gutíerrez, E. Cruz-Silva, L. P. Rajukumar, M. S. Dresselhaus, and M. Terrones, *Nano Today* **10**, 559 (2015).
3. Y. Xiao, M. Zhou, M. Zeng, and L. Fu, *Adv. Sci.* **6**, 1801501 (2019).
4. Y. Liu, N. O. Weiss, X. Duan, H. C. Cheng, Y. Huang, and X. Duan, *Nat. Rev. Mater.* **1**, 16042 (2016).
5. T. D. Thanh, N. D. Chuong, H. V. Hien, T. Kshetri, L. H. Tuan, N. H. Kim, and J. H. Lee, *Prog. Mater. Sci.* **96**, 51 (2018).
6. N. Mounet, M. Gibertini, P. Schwaller, A. Campi, D. Merkys, A. Marrazzo, T. Sohier, I. E. Castelli, A. Cepellotti, G. Pizzi, and N. Marzari, *Nature Nanotech.* **13**, 246 (2018).
7. M. A. Susner, M. Chyasnavichyus, M. A. McGuire, P. Ganesh, and P. Maksymovych, *Adv. Mater.* **29**, 1602852 (2017).
8. W. Klingen, R. Ott, H. Hahn, and Z. Anorg. *Allg. Chem.* **396**, 271 (1973).
9. G. Ouvrard, R. Brec, and J. Rouxel, *Mater. Res. Bulletin* **20**, 1181 (1985).
10. F. Boucher, M. Evain, and R. Brec, *J. Alloys Compd.* **215**, 63 (1994).
11. P. Fuentealba, C. Olea, H. Aguilar-Bolados, N. Audebrand, R. C. de Santana, C. Doerenkamp, H. Eckert, C. J. Magon, and E. Spodine, *Phys. Chem. Chem. Phys.* **22**, 8315 (2020).
12. C. Calareso, V. Grasso, and L. Silipigni, *J. Appl. Phys.* **82**, 6228 (1997).
13. R. Brec, D. M. Schleich, G. Ouvrard, A. Louisy, and J. Rouxel, *Inorg. Chem.* **18**, 1814 (1979).
14. D. Yang, P. Westreich, and R. Frindt, *J. Solid State Chem.* **166**, 421 (2002).
15. K.-Z. Du, X.-Z. Wang, Y. Liu, P. Hu, M. I. B. Utama, C. K. Gan, Q. Xiong, and C. Kloc, *ACS Nano* **10**, 1738 (2016).
16. E. Lifshitz, A. Francis, and R. Clarke, *Solid State Commun.* **45**, 273 (1983).
17. F. Boucher, M. Evain, and R. Brec, *Acta Cryst. B* **51**, 952 (1995).
18. C. Sourisseau, R. Cavagnat, M. Evain, and R. Brec, *J. Raman Spectrosc.* **27**, 185 (1996).
19. J. Liu, X.-B. Li, D. Wang, W.-M. Lau, P. Peng, and L.-M. Liu, *J. Chem. Phys.* **140**, 054707 (2014).
20. H. Xiang, B. Xu, Y. Xia, J. Yin, and Z. Liu, *RSC Adv.* **6**, 89901 (2016).
21. A. Hashemi, H.-P. Komsa, M. Puska, and A. V. Krasheninnikov, *J. Phys. Chem. C* **121**, 27207 (2017).
22. A. V. Krukau, O. A. Vydrov, A. F. Izmaylov, and G. E. Scuseria, *J. Chem. Phys.* **125**, 224106 (2006).
23. J. P. Perdew, K. Burke, and M. Ernzerhof, *Phys. Rev. Lett.* **77**, 3865 (1996).
24. R. Dovesi, A. Erba, R. Orlando, C. M. Zicovich-Wilson, B. Civalleri, L. Maschio, M. Rérat, S. Casassa, J. Baima, S. Salustro, and B. Kirtman, *WIREs Comput. Mol. Sci.* **8**, e1360 (2018).
25. D. V. Oliveira, J. Laun, M. F. Peintinger, and T. Bredow, *J. Comput. Chem.* **40**, 2364 (2019).
26. H. J. Monkhorst and J. D. Pack, *Phys. Rev. B* **13**, 5188 (1976).
27. Y. Zhao and D. G. Truhlar, *Theor. Chem. Account.* **120**, 215 (2008).
28. R. S. Mulliken, *J. Chem. Phys.* **23**, 1833 (1955).
29. Y. Hinuma, G. Pizzi, Y. Kumagai, F. Oba, and I. Tanaka, *Comput. Mater. Sci.* **128**, 140 (2017).
30. M. I. Aroyo, D. Orobengoa, G. de la Flor, E. S. Tasci, J. M. Perez-Mato, and H. Wondratschek, *Acta Crystallogr. A* **70**, 126 (2014).
31. A. Erba, M. Ferrabone, R. Orlando, and R. Dovesi, *J. Comput. Chem.* **34**, 346 (2013).

32. F. Pascale, C. M. Zicovich-Wilson, F. López Gejo, B. Civalleri, R. Orlando, and R. Dovesi, *J. Comput. Chem.* **25**, 888 (2004).
33. A. J. Jackson, J. M. Skelton, C. H. Hendon, K. T. Butler, and A. Walsh, *J. Chem. Phys.* **143**, 184101 (2015).
34. V. Zhukov, F. Boucher, P. Alemany, M. Evain, and S. Alvarez, *Inorg. Chem.* **34**, 1159 (1995).
35. R. A. Evarestov and A. Kuzmin, *J. Comput. Chem.* **41**, 1337 (2020).
36. K. Momma and F. Izumi, *J. Appl. Crystallogr.* **44**, 1272 (2011).

Дослідження з перших принципів методом LCAO фаз $CdPS_3$ при низькій та кімнатній температурах

Alexei Kuzmin

Електронну та атомну структуру об'ємної шаруватої (2D) ван-дер-ваальсової сполуки $CdPS_3$ вивчено у низькотемпературній фазі $R3$, а також у фазі $C2/m$ при кімнатній температурі з використанням розрахунків з перших принципів методом періодичної лінійної комбінації атомних орбіталей з гібридним метаобмінним кореляційним функціоналом M06. Результати розрахунку добре узгоджуються з експериментальними кристалографічними параметрами. Отримана ширина непрямої забороненої зони E_g = 3,4 еВ для моноклінної фази $C2/m$ при кімнатній температурі є близькою до експериментальної величини, стосовно низькотемпературної тригональної фази $R3$ передбачається ширина непрямої забороненої зони E_g = 3,3 еВ. Вплив гідростатичного тиску на ширину забороненої зони в обох фазах досліджено у діапазоні тисків від 0 до 40 ГПа. В обох випадках залежність ширини забороненої зони від тиску має максимум, але при різних тисках. У фазі $R3$ ширина забороненої зони досягає максимального значення ~ 4 еВ при ~ 30 ГПа, тоді як у фазі $C2/m$ максимальне значення ~3,6 еВ досягається вже при ~ 8 ГПа.

Ключові слова: $CdPS_3$, шарувата сполука, електронна структура, розрахунки з перших принципів, високий тиск.